JACS
JOURNAL OF THE AMERICAN CHEMICAL SOCIETY
Article
pubs.acs.org/JACS

Dynamics of Uranyl Peroxide Nanocapsules

May Nyman*[,†,‡] and Todd M. Alam[†]

[†]Sandia National Laboratories, Albuquerque, New Mexico 87185, United States
[‡]Department of Chemistry, Oregon State University, Corvallis, Oregon 97331, United States

Supporting Information

ABSTRACT: Discrete aqueous metal oxide polyionic clusters that include aluminum polycations, transition-metal polyoxometalates, and the actinyl peroxide clusters have captivated the interest of scientists in the realm of both their fundamental and applied chemistries. Yet the counterions for these polycations or polyanions are often ignored, even though they are imperative for solubility, crystallization, purification, and even templating cluster formation. The actinyl peroxide clusters have counterions not only external, but internal to the hollow peroxide capsules. In this study, we reveal the dynamic behavior of these internal alkali counterions via solid-state and liquid NMR experiments. These studies on two select cluster geometries, those containing 24 and 28 uranyl polyhedra, respectively, show that the capsules-like clusters are not rigid entities. Rather, the internal alkalis both have mobility inside the capsules, as well as exchange with species in the media in which they are dissolved. The alkali mobilities are affected by both what is inside the clusters as well as the composition of the dissolving medium.

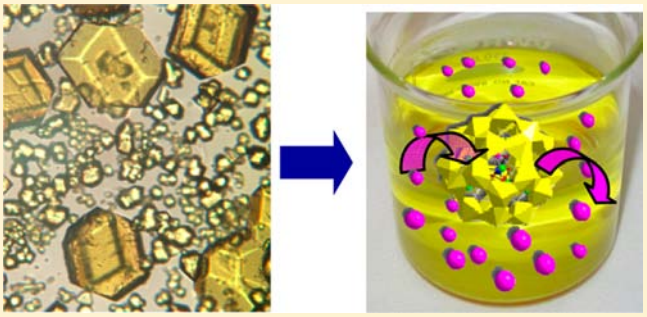

INTRODUCTION

When considering manipulation of ionic clusters such as polyoxometalates[1] or aluminum polycations,[2] the counterions are of paramount importance in both applications and fundamental chemistry, but are often neglected in the chemical literature. Actinyl peroxide polyoxometalate-like clusters are a relatively recent addition to the metal−-oxo cluster landscape of the Periodic Table. Since the seminal discovery of uranyl and neptunyl peroxide clusters in 2005,[3] approximately 60 cluster topologies have been subsequently reported by the Burns group.[4,5] Similar to the V, Nb, Ta, Mo, and W transition-metal polyoxometalates (TM-POMs), the surface of these actinyl POM clusters is terminated by an "*yl*" oxygen at every metal cation (U^{6+}/Np^{5+}), they are anionic, and they are crystallized as alkali-metal salts. They differ from TM-POMs in that the diuranyl, UO_2^{2+}, provides an internal "*yl*"-terminated surface, which results in a capsule-like topology, and these *yl* oxygens bind a shell of alkali cations internal to the anionic uranyl peroxide shell. The internal alkali cations provide very important structural and aqueous stability to the capsules in two ways: (1) They reduce the high anionic charge of the uranyl-peroxide shell; and (2) they reside inside square, pentagonal, and hexagonal faces of the uranyl-peroxide shell, perhaps stabilizing these features and even initially templating their assembly.[6,7] Moreover, inspection of a variety of reported cluster topologies suggests there is clearly size selectivity: Li^+ is located inside square faces,[3] Na^+ and K^+ prefer pentagonal faces,[8,9] and Rb^+ and Cs^+ are hosted inside hexagonal faces.[3,10,11] Furthermore, the pentagonal faces bind K, Rb, and Cs outside the capsules, through five $A^+-O_{peroxide}$ bonds (A = K, Rb, Cs).[10]

While there has been substantial focus on the origin of the many varieties of capsule geometries, minimal attention has been devoted to these alkalis, both external and internal. Yet, the alkalis are essential for assembly, stabilization, crystallization, and dissolution of the capsules. Understanding and controlling these processes will lead to the ability to manipulate the capsules in solution, and ultimately drive the fundamental science toward utility in separations, understanding nuclear fuel corrosion and actinide transport in the environment, and nanoscale assembly for nuclear fuel applications.

We present herein a survey study of the behavior of the internal cations, sodium in particular, of two uranyl clusters dissolved in water: U_{28} ($[UO_2(O_2)_{1.5}]_{28}^{28-}$) and U_{24} ($[UO_2(O_2)(OH)_2]_{24}^{24-}$), both illustrated in Figure 1 with an emphasis on their internal ionic species. Solid-state and solution ^{23}Na and ^{133}Cs NMR (nuclear magnetic resonance) spectroscopies provide remarkably accurate agreement with solid-state structure, and detailed information about the exchange of the alkalis between the inside of the capsule and the surrounding aqueous medium. These studies demonstrate that the capsules are not rigid entities. Rather, they are dynamic and exhibit mobility inside the capsules, as well as exchange ions in response to their aqueous environment.

Received: August 31, 2012
Published: November 20, 2012

   dx.doi.org/10.1021/ja308673f | J. Am. Chem. Soc. 2012, 134, 20131−20138

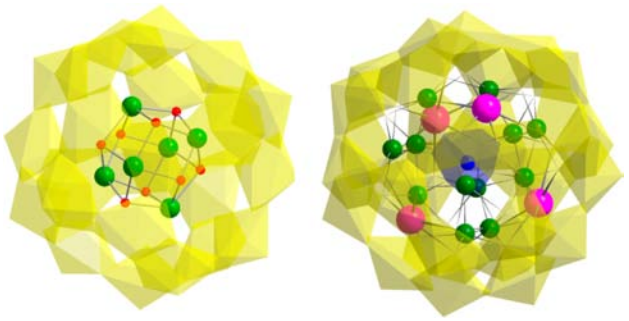

Figure 1. Views of the Na-containing uranyl peroxide nanocapsules emphasizing the internal species: Left is Na−U_{24} with a $Na_6(H_2O)_8$ cluster inside a $[UO_2(O_2)(OH)_2]_{24}^{24-}$ shell. Right is Ta−NaCsU_{28} or Nb−NaRbU_{28} with Na, Cs, or Rb and TaO_8 or NbO_8 inside a $[UO_2(O_2)_{1.5}]_{28}^{28-}$ shell. Yellow polyhedra are uranyl-centered, green spheres are Na^+, pink spheres are Cs/Rb^+, red spheres are water, and the blue polyhedron is the central Ta$[O_2]_4$ or Nb$[O_2]_4$ in U_{28}.

EXPERIMENTAL SECTION

The synthesis of Ta−NaCs−U_{28} and Nb−NaRbU_{28} was previously reported.[12] For the synthesis of Na−U_{24}, the lithium monomer, $Li_4UO_2(O_2)_3{\cdot}10H_2O$,[13] is first synthesized. One millimole of uranyl nitrate hexahydrate is dissolved in 6 mL of DI water. An 80 mL beaker containing a stir bar is placed in an icebath and charged with 3 mL of 30% H_2O_2 plus 4 mL of 4 M LiOH. While stirring, the uranyl nitrate solution is added to the peroxide/LiOH aqueous mixture, and a bubbly orange solution is obtained. While continuing to stir rapidly, ethanol is added via a squirt bottle, and the solution goes from clear orange to a murky yellow slurry as the monomer salt is precipitated. The monomer salt is then isolated by vacuum filtration on filter paper and washed with more ethanol. The beaker (containing remaining monomer salt that was not readily removed) is then charged with 50 mL of DI water, and the remainder of the isolated monomer is added to the solution with stirring. The lithium monomer solution is left stirring at room temperature for 2−4 h (can also be left overnight without detriment to the synthesis). The color changes from orange to yellow, indicating formation of the U_{24} capsule. Sodium acetate (0.1 g) is dissolved in a minimal amount of water and added to the Li−U_{24} solution. The beaker is left inside the fumehood to allow water to evaporate. After 1 day, well-faceted crystals are observed, and harvested after several days. Yield is around 0.3 g, ∼30% based on uranium. Na−U_{24} was characterized by several methods to confirm the single-crystal structure (below) matches the bulk, and to confirm the purity of the bulk. Powder X-ray diffraction shows good crystallinity and matches that calculated from the single-crystal X-ray data (see the Supporting Information). Thermogravimetry to 700 °C converts Na−U_{24} to $(Na_{0.89}Li_{0.11})_2U_2O_7$ (determined by powder X-ray diffraction) with 21% weight loss, which agrees precisely with the calculated amount for:

$$Li_2Na_{16}[Na_6(H_2O)_8][UO_2(O_2)(OH)]_{24}{\cdot}72H_2O \rightarrow 24[(Na_{0.89}Li_{0.11})_2U_2O_7]$$

X-ray Structure of Na−U_{24}. Single-crystal X-ray data were collected at −80 °C on a Bruker AXS SMART-CCD diffractometer with graphite monochromated Mo Kα (0.71073 Å) radiation. Data collection and reduction were carried out with SMART 5.054 (Bruker, 1998) and SAINT 6.02 (Bruker, 2001) software, respectively. Numerical absorption correction from face indexing was applied. The structures were solved by Direct Methods (program SIR97) and refined by full matrix least-squares on F^2 (SHELX97). All subsequent structure solution and refinement were performed within the WinGX system. Compound **Na−U_{24}**: $Li_2Na_{16}[Na_6(H_2O)_8][UO_2(O_2)(OH)]_{24}{\cdot}72H_2O$, $H_{184}O_{200}Li_2Na_{22}U_{24}$, FW = 9599.8; monoclinic, $C2/m$ (No. 12), a = 26.184(2) Å, b = 26.175(2) Å, c = 18.415(2) Å, β = 132.259(1)°, V = 9341(2) Å^3, Z = 2, ρ_{calcd} = 3.345 g cm^{-3}; μ(Mo Kα) = 20.9 mm^{-1}; 1.41 ≤ θ ≤ 25.00°, $R_1(I > 2\sigma(I))$ = 0.0316, wR_2 $(I > 2\sigma(I))$ = 0.0831. The data have been deposited with the ICSD, Fiz-Karlsruhe, Deutschland (CSD-424819).

Aqueous solutions for NMR were prepared with the concentration 0.2 mM U_{24} or U_{28} in 1 mL of D_2O (approximately 0.020 g of uranyl cluster salt per milliliter of D_2O).

NMR Experiments. The solid-state MAS NMR spectra were obtained on a Bruker AVANCE-I instrument operating at 105.84 and 52.49 MHz for ^{23}Na and ^{133}Cs, respectively. Spectra were obtained on a 4 mm broadband MAS probe spinning between 10 and 12.5 kHz. A standard single pulse Bloch decay sequence with high power ^{1}H decoupling was employed. The multiple quantum (MQ) MAS spectrum was obtained using the two pulse zero quantum filtered triple quantum (3Q) sequence, followed by a shear transformation. The variable-temperature solution ^{23}Na NMR spectra were obtained on a Bruker Avance III instrument operating at 132.3 MHz using a 5 mm broadband probe. All NMR analyses used quartz tubes to eliminate the ^{23}Na background signal of common borosilicate NMR tubes. The ^{23}Na chemical shift was referenced to the external secondary standard 1 M NaCl δ = 0, while the ^{133}Cs chemical shifts were referenced to 1 M CsCl δ = 0. Solid-state spectral simulations were performed using the DMFIT software package,[14] including the introduction of Czjzek distribution to describe the Na quadrupolar interactions. Analysis of the variable-temperature exchange spectra utilized the dynamic line shape simulation software package WINDNMR-Pro.[15]

RESULTS AND DISCUSSION

Synthesis. For these studies, it is extremely important to begin with a salt whose internal and external cations are all accounted for and quantified in the solid state; thus we utilized two previously reported formulations of U_{28},[12] and a new formulation of U_{24}. The U_{28} cluster contains a central anion, in addition to the outer uranyl-peroxide shell and a well-defined inner alkali shell. With the proper choice of (1) internal cations, K^+ in the pentagonal faces and Rb/Cs^+ in the hexagonal faces, (2) central anion, $Ta/Nb(O_2)_4^{3-}$ that matches the tetrahedral symmetry of the capsule, and (3) external charge-balancing cations, Cs/Rb^+ for rapid precipitation, maximum yields approaching 80% and high purity of material can be obtained. Dissolution of the previously reported U_{28} analogues[10] $Cs_{16}[Ta(O_2)_4K_{12}Cs_4\{UO_2(O_2)_{1.5}\}_{28}]H_2O$ (Ta-KCsU_{28}) and $Rb_{12.5}K_{3.5}[Nb(O_2)_4K_{12}Cs_4\{UO_2(O_2)_{1.5}\}_{28}]{\cdot}H_2O$ (Nb-KRbU_{28}) in sodium hydroxide or sodium acetate solution results in growth of well-formed dodecahedral-shaped yellow crystals within a day of preparing the solution. Single-crystal X-ray diffraction of these phases reveals that the 12 internal K^+ in the pentagonal windows are replaced entirely with Na^+, and the external cations are a nonselective mixture of Na^+ and K^+, the ratios of which were best estimated by a combination of optimization of crystallographic thermal parameters, energy dispersive spectroscopy (EDS) for compositional analysis, and ^{23}Na solid-state NMR analysis. These combined methods provided formulas of $Na_6K_9[Ta(O_2)_4Cs_4Na_{12}\{(UO_2)(O_2)_{1.5}\}_{28}]{\cdot}6H_2O$ (Ta-NaCsU_{28}; CSD-423772) and $K_{7.5}Na_{7.5}[Nb(O_2)_4Na_{12}Rb_4\{(UO_2)(O_2)_{1.5}\}_{28}]{\cdot}12H_2O$ (Nb-NaRbU_{28}; CSD-423773).[12] The U_{24} analogue reported here for the first time has a simpler formula featuring almost purely Na^+ cations both inside and outside the capsule in the crystalline lattice: $Li_2Na_{16}[Na_6(H_2O)_8][UO_2(O_2)(OH)]_{24}{\cdot}72H_2O$ (Na−U_{24}; CSD-424819). The lithium is tetrahedrally coordinated with water in the crystalline lattice, and its presence was confirmed by ^{7}Li NMR; a peak is observed around 0 ppm for an aqueous solution of Na−U_{24} salt. The synthesis of Na−U_{24} is extremely easy and reproducible. The

prior reported $Li_4UO_2(O_2)_3{\cdot}10H_2O$ monomer salt[13] dissolved in neat water produces a clear orange solution, which turns yellow upon stirring for ~2 h at room temperature, indicating formation of the nanocapsules (Li−U_{24}). At this point, sodium acetate is added, and after several hours, well-faceted crystals grow, with a yield around 30%. Unlike the Li−U_{24} analogue previously reported,[3] all alkali cations, both inside and outside, can be accurately located.

Structural Descriptions. We have reported isostructural Nb−NaRbU_{28} and Ta−NaCsU_{28} recently, and discussed these in some detail, especially in comparison to computational studies describing the disordered central $Ta(O_2)_4^{3-}$ and $Nb(O_2)_4^{3-}$.[12] Briefly, both salts crystallize in the cubic $I\bar{4}3m$ space group. Both consist of a spherical shell composed of 28 $UO_2(O_2)_3^{4-}$ hexagonal bipyramids that share the peroxide ligand edge, and are linked in an arrangement that produces 12 pentagonal windows and four hexagonal windows; the latter are arranged tetrahedrally in the spherical shell. Each pentagonal window hosts a Na^+ cation, while each hexagonal window binds the Rb^+ or Cs^+. The Ta−NaCsU_{28} analogue has a considerably smaller unit cell (7345(17) Å^3) than the Rb−NaRbU_{28} (8162(17) Å^3) analogue due to both fewer water molecules in the ionic lattice, as well as the unusual manner in which the Ta−NaCsU_{28} anions are linked to each other. The Cs^+-cations that reside inside the hexagonal windows actually connect to adjacent clusters through a 3.3 Å U═O_{yl}−Cs bond resulting in a supertetrahedral network (Figure S1). The Rb^+-cations are apparently too small to allow this sort of connectivity, in that this bonding mode is not observed for Nb−NaRb−U_{28}.

Na−U_{24} crystallizes in monoclinic space group $C2/m$. The uranyl peroxide shell is identical to that reported originally by Burns et al.,[3] consisting of 24 $UO_2(OH)_2(O_2)_2^{4-}$ polyhedra with the hydroxyl ligands in a *cis*-arrangement. The capsule is composed of six square rings and eight hexagonal rings. Encapsulated inside the cluster is a $Na_6(H_2O)_8$ cluster: the Na^+-cations sit inside the square windows, and the water molecules reside directly underneath the hexagonal windows (Figure 1). The Na^+ cations bond to four internal −O_{yl} oxygens of the square face, with bond lengths ranging from 2.369(2) to 2.594(1) Å, and the bonds to the internal water molecules range from 2.386(1) to 2.688(1) Å. The bonding mode of these internal Na^+ cations to the uranyl shell resembles that of the Li^+ cations inside the Np_{24} analogue reported previously. The water molecules reside approximately 3 Å from the O_{yl} oxygens of the hexagonal window.

NMR Studies in the Solid and Liquid States. The two U_{28} salts and the U_{24} salt that are the subjects of this Article are all readily soluble in neat water, without the addition of any added electrolyte. The uranyl shells of the capsules remain intact in solution; they can be crystallized back out of solution with the addition of excess sodium, but never completely so, due to the high solubility and perhaps some cluster alteration resulting from the internal−external species exchanges that take place as described below. Some preliminary studies on the alteration behavior of both U_{24} and U_{28} clusters utilizing ^{17}O NMR have been carried out. These indicate that excess peroxide and alkali in the solution with the clusters increase their stability, and more detailed studies will be forthcoming.[16] While the uranyl shells retain their structural integrity, we observe dynamic behavior of the alkalis between the capsules and the aqueous media. In this sense, the capsules behave like nano ion-exchangers. We first turn our attention to the solid state to both confirm structure and benchmark the solution-phase peaks. Figure 2a shows a ^{23}Na solid-state MAS NMR (magic-angle spinning nuclear magnetic resonance) spectrum

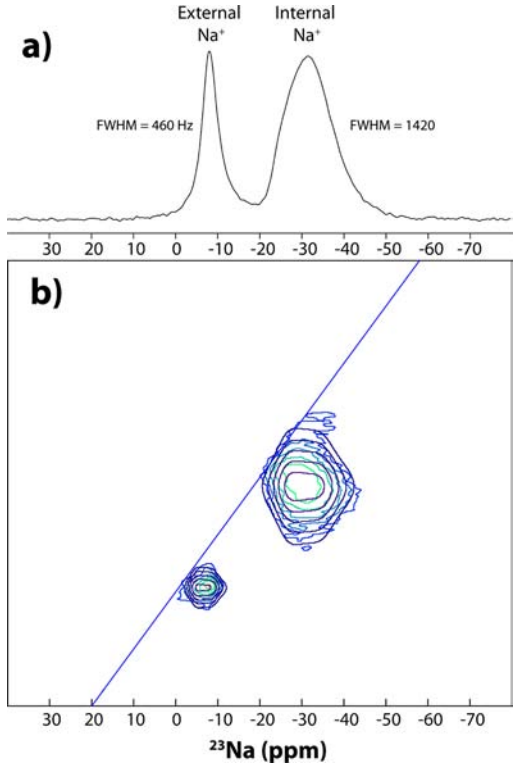

Figure 2. (a) 1D ^{23}Na MAS NMR spectrum and (b) 2D ^{23}Na MQ-MAS NMR spectrum of the Ta−NaCsU_{28} salt at 25 °C.

of Ta−NaCsU_{28}. The broad peak of Na^+ internal to capsule (~ −32 ppm, fwhm = 1420 Hz) is 65% of the total integrated spectrum, and the sharper peak of the external Na^+ (−8.1 ppm, fwhm = 460 Hz) is 35%, agreeing with the 2:1 ratio of internal to external Na^+ environments determined by compositional analysis and X-ray structure refinement. The peak at −32 ppm of the 12 Na^+ cations inside the pentagonal rings cannot readily be fit as a single peak. Rather this resonance represents a large distribution of chemical shifts (σ(CS) ≈ 10 ppm) and a limited range of quadrupolar coupling constants (QCC_{max} = 1.2 MHz, σ(QCC) = 0.6 MHz), suggesting significant distortion or disorder in this Na crystallographic site. The distribution in QCC has been modeled using the Czjzek distribution with a Gaussian isotropic model (GIM, d = 5).[17−19] The distribution in the chemical shift and QCC can also be seen in the multiple quantum MQ-MAS spectrum (Figure 2b) and corresponding simulation (black contours). These NMR results agree well with the structural and computational interpretation;[12] both show disorder of the Na-cations inside the capsule. The peroxide ligands of the $Ta(O_2)_4^{3-}$ central anion have three orientations, which results in a structural representation of a triangle of three two-thirds occupied oxygen atoms. Correlated with this is the disorder of the internal Na^+ cations: they sit in two positions with two-third and one-third occupancy at −80 °C, the temperature at which the X-ray data were collected. The prior computational studies,[12] also predicting this disorder, were performed at 0 K. Thus with an increase to room temperature at which the NMR experiments were executed, the two rigid sites for sodium in the pentagonal window identified by X-ray diffraction and computational studies may in fact be a

dx.doi.org/10.1021/ja308673f | J. Am. Chem. Soc. 2012, 134, 20131−20138

distribution between the two positions, as suggested by the ^{23}Na MAS NMR. The ^{23}Na MAS NMR spectrum of Nb−$NaRbU_{28}$ is comparable and shown in the Supporting Information (Figure S5).

The ^{23}Na MAS NMR spectrum of Na−U_{24} is shown in Figure 3. Similar to the U_{28} analogues, there are two peaks: one

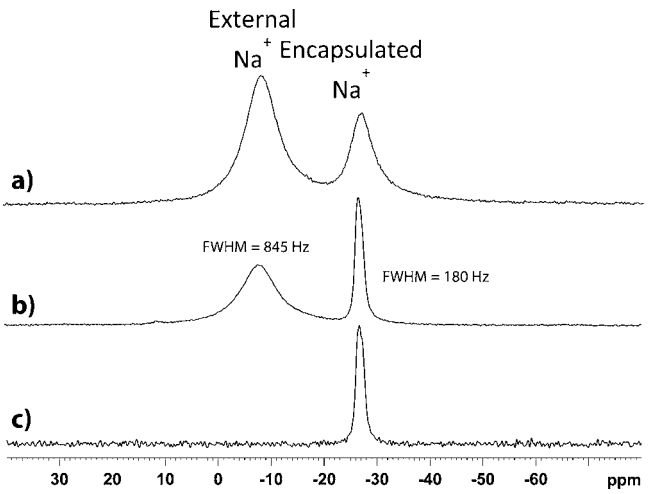

Figure 3. 1D ^{23}Na MAS NMR spectra of Na−U_{24} obtained under (a) no ^{1}H decoupling, (b) ^{1}H decoupling, and (c) ^{1}H−^{23}Na CPMAS condition for the Na−U_{24} cluster.

for external Na (−7.9 ppm, fwhm = 845 Hz, 70%) and one for the Na inside the capsule (−26.8 ppm, fwhm = 180 Hz, 30%) with ratios that approximately agree with the X-ray structure. However, in this case, the external Na-peak is actually broader than the internal Na-peak, with the line width of the external Na-peak nearly doubled between the U_{28} analogues and Na−U_{24}. The sharp internal ^{23}Na-peak (~8 times narrower) for U_{24} as compared to that of U_{28} arises from either an increased mobility of Na inside the Na−U_{24} cluster or a reduced distribution of Na environments for this salt. Proton decoupling and cross-polarization experiments both reveal the close and tightly bound association of water with the sodium cations of the encapsulated $Na_6(H_2O)_8$ cluster; see Figure 3. Although there are abundant H_2O molecules in the crystalline lattice on the outside of Na−U_{24} capsules that are bonded to the external, charge-balancing Na-cations with distances ranging from 2.291(1) to 2.975(1) Å, the crystals readily dehydrate, indicating the water is not tightly held in the lattice. In addition, these external waters may have significant mobility, reducing the efficiency of the ^{1}H−^{23}Na dipolar coupling with the external Na, in contrast to the encapsulated Na, which has significant dipolar coupling. These differences explain why the external Na-cations do not exhibit the same cross-polarization or proton-decoupling behavior as that of the internal encapsulated Na-cations.

Solution-phase ^{23}Na NMR of the dissolved U_{28} and U_{24} capsules revealed the dynamic behavior of the Na^+ cations in Ta−$NaCsU_{28}$, Nb−$NaRbU_{28}$, and Na−U_{24}. Figure 4 shows the ^{23}Na spectrum of Ta−$NaCsU_{28}$ in neat water, as it is heated from 25 to 90 °C (the Nb−$NaRbU_{28}$ appears similar and is shown in the Supporting Information). The external and internal sodium peaks are shifted from those observed in the solid state and shift further with heating. For instance, the room temperature external ^{23}Na peak is located at −0.4 ppm, and the broad internal ^{23}Na peak is at −23 ppm. With increasing

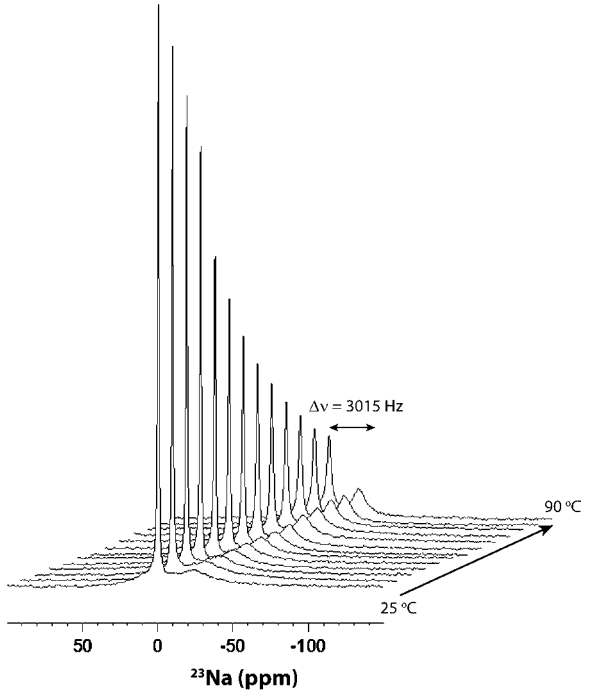

Figure 4. Variable-temperature solution ^{23}Na NMR spectra of Ta−$NaCsU_{28}$.

temperature, the exchange rate between the capsule and the external Na increases, resulting in the broadening of the external peak and the reduction in the chemical shift difference between the two different species. The observation of two distinct ^{23}Na resonances, which do not coalesce for this temperature range, demonstrates that the exchange rate must be slower than the peak separation (rate $\ll \Delta\nu \approx 3000$ Hz). It should be noted that for Na environments not undergoing exchange, increasing the temperature would result in line narrowing, as the quadrupolar relaxation becomes less efficient due to increased molecular tumbling. The observation of broadening for the external Na resonance ($\delta \approx -0.4$ ppm) with increasing temperature proves that these Na^+ are indeed undergoing exchange with the Na^+ internal to the capsules. It should also be noted that for the U_{28} complexes the encapsulated Na resonance shows a complicated change in line shape with increasing temperature, and appears to include the overlap of several different types of dynamic environments. This is consistent with the distribution of environments observed in the solid state, and suggests that the exchange process may involve multiple steps. As a first approximation, the exchange process is modeled as a simple internal/external two-site exchange in the following discussion.

The variation of the line width of the hydrated external Na resonance as a function of temperature (Figure S5, Supporting Information) has been used to estimate the Na exchange rate Nb−$NaRbU_{28}$ and Ta−$NaCsU_{28}$ that are (a) dissolved in neat D_2O and (b) dissolved in 0.085 M sodium acetate solution (excess Na).[20] The exchange rates were fit to the Eyring equation in Figure 5a, allowing the determination of the free energy of activation ($\Delta G^{\ddagger}$), enthalpy of activation ($\Delta H^{\ddagger}$), and entropy of activation ($\Delta S^{\ddagger}$) for the U_{28} capsules.[21] Table 1 summarizes these results.

The rate of exchange of sodium between the external solution and the Nb−$NaRbU_{28}$ capsule is more rapid (smaller $\Delta G^{\ddagger}$) than the exchange rate observed for the Ta−$NaCsU_{28}$

dx.doi.org/10.1021/ja308673f | J. Am. Chem. Soc. 2012, 134, 20131−20138

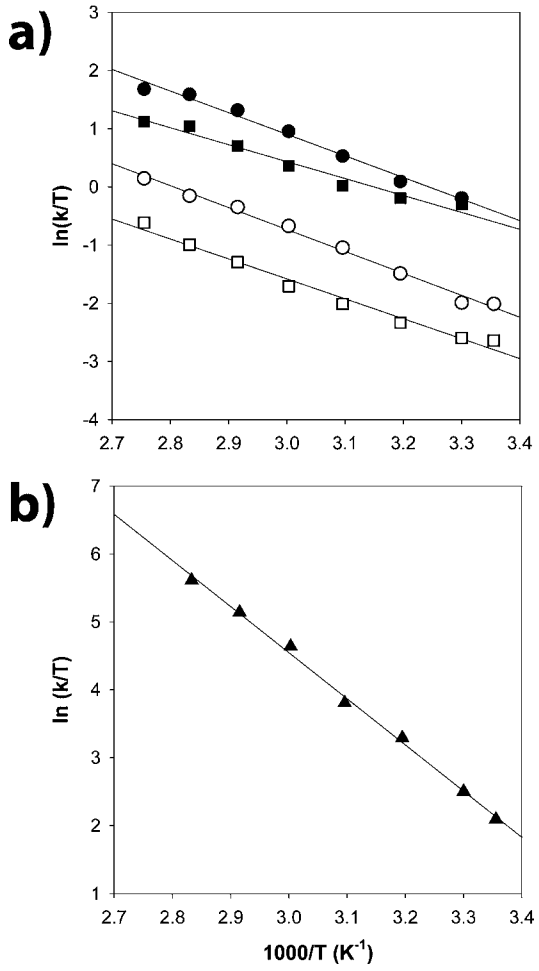

Figure 5. Exchange rate temperature variation from ^{23}Na NMR analysis for (a) the Nb−NaRbU$_{28}$ (●) and Ta−NaCsU$_{28}$ (■) clusters in water, and in a 0.085 M sodium acetate solution (○, □), and (b) the Na−U$_{24}$ cluster in water.

Table 1. Activation Enthalpies, Entropies, and Free Energies for the U$_{28}$ and U$_{24}$ Complexes Obtained from ^{23}Na NMR

sample	$\Delta H^{\ddagger}$ (kJ mol^{-1})	$\Delta S^{\ddagger}$ (J mol^{-1} K^{-1})	$\Delta G_{298K}{}^{\ddagger}$ (kJ mol^{-1})
Nb−NaRbU$_{28}$	30.9 (r^2 = 0.9863)	−97.4	+59.9
Ta−NaCsU$_{28}$	24.2 (r^2 = 0.9702)	−121.3	+60.3
Nb−NaRbU$_{28}$ (excess Na)	31.3 (r^2 = 0.9923)	−109.5	+63.9
Ta−NaCsU$_{28}$ (excess Na)	28.5 (r^2 = 0.9818)	−125.2	+65.8
Na−U$_{24}$	56.5 (r^2 = 0.997)	+11.0	+53.2

capsule, with and without excess sodium salt added to the solution. Second, the exchange rates in both complexes were slowed (a larger $\Delta G^{\ddagger}$) by the addition of excess sodium to the system. The slowing of the exchange with added external Na$^+$ suggests that Na$^+$ exiting the capsule is the rate-determining step of the exchange. The negative entropy is discussed below in comparison to the U$_{24}$ capsule.

To further understand the relative rates of Na$^+$ exchange of the two U$_{28}$ analogues, we next turn our attention to correlated behavior of Cs$^+$. Figure 6 shows the variable-temperature ^{133}Cs NMR spectrum of Ta−NaCsU$_{28}$ between 30 and 90 °C. The sharp peak at −23 ppm is likely a small amount of external Cs$^+$, while the broad peak at +23 ppm corresponds with the

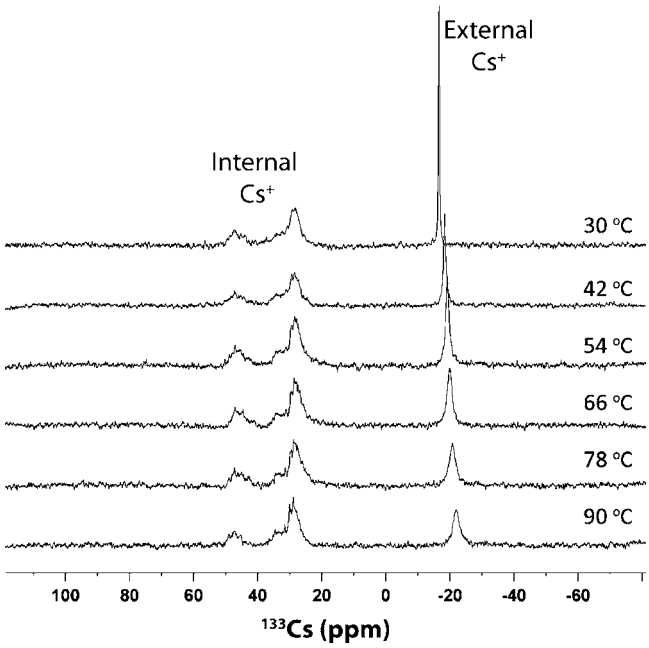

Figure 6. Variable-temperature solution ^{133}Cs NMR of Ta−NaCsU$_{28}$.

encapsulated Cs$^+$. Free, fully hydrated Cs$^+$ resonates at δ = 0 ppm, suggesting that the external Cs is not free in solution, but remains associated with the U$_{28}$ complex. With heating, the "external" Cs$^+$ peak clearly shifts away from the internal Cs$^+$ peak (^{133}Cs NMR chemical shifts are known to be very temperature sensitive), and broadens, which again indicates Cs is exchanging between different environments. The lack of coalescence between the internal and external Cs environments shows that this exchange process is slow on the order of the peak separation ($\Delta\nu \approx 4000$ Hz). The Eyring analysis of the broadening revealed a slightly nonlinear behavior (r^2 = 0.93), giving a $\Delta G_{298K}{}^{\ddagger} \approx 65.8$ kJ mol^{-1} ($\Delta H^{\ddagger}$ = 48.3 kJ mol^{-1} and $\Delta S^{\ddagger} = -58.7$ J mol^{-1} K^{-1}). This activation free energy is on the same order as those observed for the Na exchange in the same complex (see Table 1). The internal Cs-peak is broadened and reveals multiple resonances over a large chemical shift range that actually changes with time and heating, indicating dynamics of Cs$^+$ within the capsule environment.

The ratio of the external and internal sodium with temperature of the aqueous solution for both Nb−NaRbU$_{28}$ and Ta−NaCsU$_{28}$ begins at 30:70 internal:external. This ratio of internal:external Na$^+$ is significantly less than that in the solid state immediately upon dissolution, suggesting some sodium rapidly exits the cluster upon dissolution. This follows our understanding that dissolved species move from areas of high concentration (internal) to low concentration (external), and entropy increases. This, along with the increased asymmetry of the internal Cs chemical environments, implies the following with respect to dynamics of these alkali cations in U$_{28}$.

- It has been observed[10] that Cs$^+$ can and does exit the U$_{28}$ structure despite its large size, and heating likely increases this activity. This may take place in conjunction with a "breathing motion" of the shell, described prior for molybdate capsule-like POMs.[22]
- The higher rate (and corresponding lower activation energy) of internal to external Na$^+$ exchange for Nb-NaRbU$_{28}$ as compared to that of Ta−NaCsU$_{28}$ is likely

dx.doi.org/10.1021/ja308673f | J. Am. Chem. Soc. 2012, 134, 20131−20138

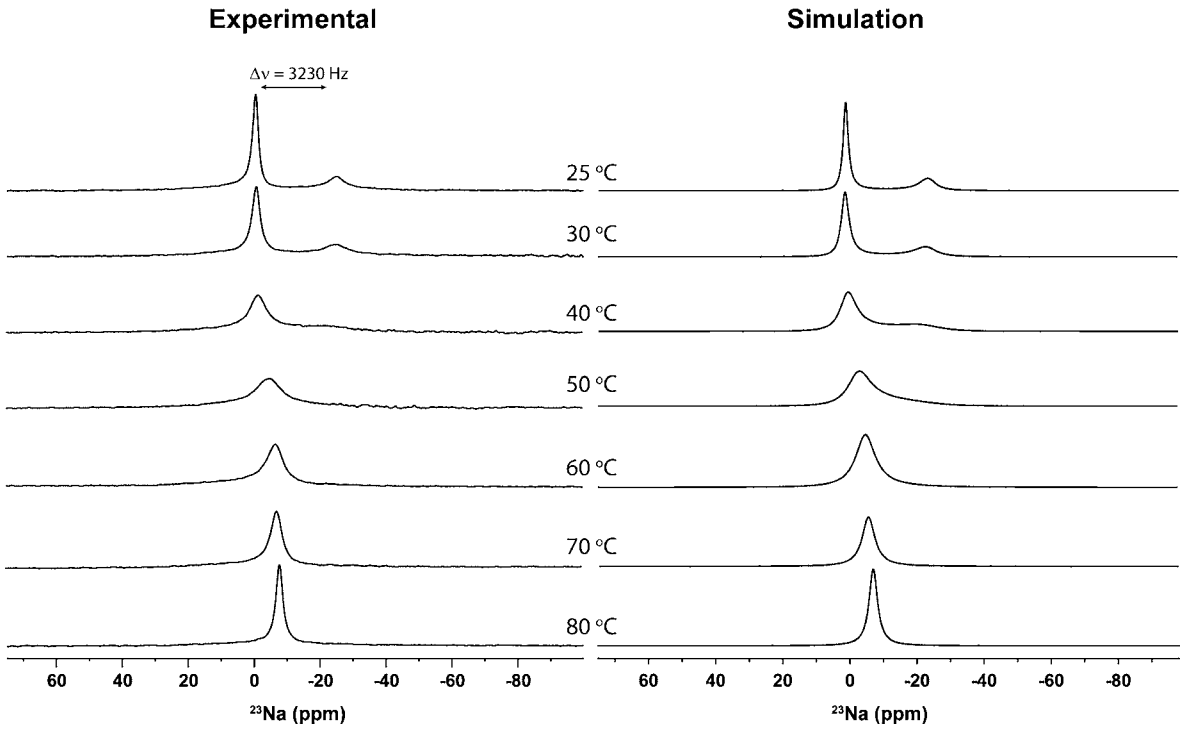

Figure 7. Variable-temperature solution ^{23}Na NMR spectra and dynamic line shape simulations for the Na−U_{24} capsule.

related to the higher mobility of smaller Rb^+, both inside the capsule and in its ability to exit the capsule.

- The motion of the Na^+ plus Rb/Cs^+ inside the capsule, and the related exchange behavior, is likely a concerted motion; that is, the cations can hop from the pentagonal to hexagonal faces and visa versa, and the central $M(O_2)_4^{3-}$ (M = Nb,Ta) anion can likely rotate. The result of this disordering of the central species is the change in the distribution of resonances in the ^{133}Cs NMR of the internal environment. In fact, it is quite possible the sodium cations exit the cluster out both the hexagonal and the pentagonal faces, and will be discussed later, in comparison to the behavior of Na−U_{24}.

Next, we turn our attention to the dynamic behavior of the Na−U_{24} capsule in solution. Figure 7 shows the two resolved Na-resonances of encapsulated (−24.6 ppm 30%) and free (−0.3 ppm 70%) sodium. Upon heating, the resonances shift toward each other and coalesce, indicating exchange between the two different Na environments has become faster than the peak separation (rate ∼3200 Hz). Simulation of this dynamic line shape behavior allowed the exchange rates to be determined as a function of temperature and is shown in Figure 5b. Clearly, the Na exchange dynamics for the Na−U_{24} cluster was far more rapid than those observed for U_{28} and is reflected in the smaller $\Delta G^{\ddagger}$ (see Table 1). The relative entropies of the five different solutions are worth some speculation, based on dynamics inside the clusters. Even though the determination of activation entropies can contain systematic errors when estimating rate constants from exchange broadened NMR spectra, and should be discussed with caution, there are distinct trends observed for the entropies in the U_{28} and U_{24} capsules. Higher negative entropies corresponded to slower exchange rates, with the extremes of $\Delta S^{\ddagger}$ = −125.2 J/mol·K for Ta−NaCsU_{28} in excess Na^+-solution and $\Delta S^{\ddagger}$ = +11 J/mol·K for Na−U_{24}. The activation entropy reflects the difference between the external environment and the transition state, with a negative transition supporting a decrease in the translational freedom perhaps due to constriction and partial channel obstruction for Na within the capsule, or an increase in the order of the Na solvent cage inside the capsules.

The faster rate of Na^+ exchange between capsule and aqueous medium for the U_{24} cluster relative to the U_{28} cluster is considerable and noteworthy. Furthermore, as noted above, the ^{23}Na MAS NMR spectra of U_{24} and U_{28} showed an 8× greater line width for Na inside U_{28} as compared to U_{24}, indicating the much lower mobility of Na inside U_{28} compared to U_{24} or a reduction in the distribution of environments. U_{24} contains a total of 14 internal species: eight Na^+ cations and six water molecules; it likewise has eight square windows and six hexagonal windows, and a capsule internal volume of 428 Å^3. This gives 30 Å^3 per non-hydrogen atom. U_{28} contains a total of 25 internal species: 16 alkali cations plus a Nb(Ta)O_8, four hexagonal windows, and 12 pentagonal windows, and a capsule internal volume of 632 Å^3, which is 25 Å^3 per non-hydrogen atom. Volume is calculated on the basis of the diameter between U−O_{yl} oxygen atoms across the center of the capsule. The volumes per internal species for U_{24} and U_{28} are not hugely different, especially considering the six water molecules inside U_{24} do carry a total of 12 protons. Therefore, higher free void space inside U_{24} is likely not the reason for its overall higher internal specie mobility and internal-to-external exchange rates. More likely, the increased dynamic exchange behavior of U_{24} relative to U_{28} is attributed to its lack of the larger alkalis (Rb and Cs) that may result in decreased overall mobility inside the capsule. Moreover, if the exit of Na^+ from both U_{28} and U_{24} can occur through any capsule window, this may also favor higher mobility for U_{24}. This is because U_{24} has more of the larger hexagonal windows than U_{28} (six vs four), and in the solid state, the larger alkalis reside in the hexagonal windows of U_{28}.

Another reason for higher Na^+ mobility in U_{24} as compared to U_{28} is perhaps the distinction of water molecules that reside

dx.doi.org/10.1021/ja308673f | J. Am. Chem. Soc. 2012, 134, 20131−20138

inside U_{24}, in conjunction with the hydroxide ligands of the uranyl peroxide hydroxide shell. Hydrogen bonding, bonding of the water to the alkalis, proton transfer between water oxygen, and mobility of these internal water molecules are all likely to play a role in the motion of the internal U_{24} species. The precise behavior of the protons, both aqua and of the hydroxyl ligands, will be described in the future by computational and experimental methods.

CONCLUSIONS

It has been noted repeatedly both through X-ray structure and computational studies that the alkali-cations in uranyl peroxide nanocapsules are well-ordered by size in the solid state, and actually play key roles in templating and crystallization. However, the current study indicates that dynamic behavior of the aqueous phase capsules results in higher entropy via disordering of the alkali-cations within the capsule, particularly if more than one alkali type is present between the solution and capsule, or if there is disequilibrium between the external and internal alkalis. It is worth comparing here the exchange behavior of the capsule-like molybdate POMs and the present study for both summary and inspiration for future studies. The pores of both the uranyl and molybdate[23,24] capsules are described as crown-ether like, and flexible in solution, allowing passage of larger cations. Muller et al.[22] describe structures of the molybdate capsules with large rare-earth cations bound in a crown-like fashion to the outside of the capsule pores, in addition to the inside: these structures were obtained from ion-exchange studies. In these studies, it is suggested that the large rare-earths first exchange with internal cations and then prevent further exchange via pore blockage. We observe this structural detail, especially with the Cs-salts of uranyl peroxide capsules, that is, cations situated both inside and outside the capsule. Finally, one considerable difference between the molybdate capsule studies and the present study is the former have been carried out in nonaqueous conditions. This drastically affects the behavior of the exchanging species. For instance, alkali exchange is considerably inhibited, due to blockage of the pores by nonaqueous solvent molecules, and inability to provide a hydrated state to the alkali after exiting the capsule.[25] The nonaqueous chemistry of the uranyl capsules is yet to be studied, but may be carried out in the future by way of appropriate countercation exchange as a means of rendering them soluble in nonaqueous solvents. These future studies will not only help in understanding the exchange processes, but will also provide a whole new solution-based realm to uranyl peroxide capsule chemistry.

Disorder and depopulation of alkalis encapsulated in the uranyl peroxide nanocapsules as we have observed in the present studies can result in a net reduction of the alkali population inside the capsules. One can then assume that such a net reduction may cause destabilization and rearrangement of the capsules because the anionic charge becomes greater. Increasing the anionic charge often results in protonation in aqueous media, as is observed in group V transition-metal polyoxometalates,[26,27] which can accelerate alternation of the initially monospecific capsules. Understanding and controlling this behavior of the uranyl peroxide nanocapsules that is likely ubiquitous is imperative for further development of their chemistry in which the counterions play a significant role. This encompasses the expanse of behaviors observed already for the transition-metal POMs such macromolecular assembly in solution,[28] transfer into nonaqueous media,[29] and labile behavior of the clusters via pH-controlled oxo-ligand exchange.[30,31] Finally applications derived from the fundamental chemistry, separations in particular, depend on a detailed understanding of the alkali counterions, both inside and outside aqueous cluster assemblies such as the uranyl nanocapsules.

ASSOCIATED CONTENT

Supporting Information

Crystallographic information file (CIF) for Na–U_{24}, and a file containing supplementary spectra and figures, referenced throughout the text. This material is available free of charge via the Internet at http://pubs.acs.org.

AUTHOR INFORMATION

Corresponding Author

may.nyman@oregonstate.edu

Notes

The authors declare no competing financial interest.

ACKNOWLEDGMENTS

This work was supported as part of the Materials Science of Actinides, an Energy Frontier Research Center funded by the Department of Energy, Office of Science, Office of Basic Energy Sciences under award number DE-SC0001089. Sandia National Laboratories is a multiprogram laboratory operated by Sandia Corp., a wholly owned subsidiary of Lockheed Martin Co., for the Department of Energy's National Nuclear Security Administration under contract DE-AC04-94AL85000.

REFERENCES

(1) Pope, M. T. *Heteropoly and Isopoly Oxometalates*; Springer-Verlag: London, 1983.
(2) Casey, W. H. *Chem. Rev.* **2006**, *106*, 1.
(3) Burns, P. C.; Kubatko, K. A.; Sigmon, G.; Fryer, B. J.; Gagnon, J. E.; Antonio, M. R.; Soderholm, L. *Angew. Chem., Int. Ed.* **2005**, *44*, 2135.
(4) Burns, P. C. *Mineral. Mag.* **2011**, *75*, 1.
(5) Nyman, M.; Burns, P. C. *Chem. Soc. Rev.* **2012**, *41*, 7354.
(6) Miro, P.; Pierrefixe, S.; Gicquel, M.; Gil, A.; Bo, C. *J. Am. Chem. Soc.* **2010**, *132*, 17787.
(7) Vlaisavljevich, B.; Gagliardi, L.; Burns, P. C. *J. Am. Chem. Soc.* **2010**, *132*, 14503.
(8) Sigmon, G. E.; Ling, J.; Unruh, D. K.; Moore-Shay, L.; Ward, M.; Weaver, B.; Burns, P. C. *J. Am. Chem. Soc.* **2009**, *131*, 16648.
(9) Sigmon, G. E.; Unruh, D. K.; Ling, J.; Weaver, B.; Ward, M.; Pressprich, L.; Simonetti, A.; Burns, P. C. *Angew. Chem., Int. Ed.* **2009**, *48*, 2737.
(10) Nyman, M.; Rodriguez, M. A.; Alam, T. M. *Eur. J. Inorg. Chem.* **2011**, 2197.
(11) Sigmon, G. E.; Weaver, B.; Kubatko, K. A.; Burns, P. C. *Inorg. Chem.* **2009**, *48*, 10907.
(12) Gil, A.; Karhanek, D.; Miro, P.; Antonio, M. R.; Nyman, M.; Bo, C. *Chem.-Eur. J.* **2012**, *18*, 8340.
(13) Armstrong, C. R.; Nyman, M.; Shvareva, T.; Sigmon, G. E.; Burns, P. C.; Navrotsky, A. *Proc. Natl. Acad. Sci. U.S.A.* **2012**, *109*, 1874.
(14) Massiot, D.; Fayon, F.; Capron, M.; King, I.; LeCalvé, S.; Durand, B. A. O.; Bujoli, B.; Gan, Z.; Hoatson, G. *Magn. Reson. Chem.* **2002**, *40*, 70.
(15) Line-shape simulations were performed with the computer program WINDNMR: Reich, H. J. *J. Chem. Educ. Software* **1996**, *3D*, 2; http://www.chem.wisc.edu/areas/reich/plt/windnmr.htm.
(16) Personal communication with: Casey, W. H., UC Davis.
(17) Neuville, D. R.; Cormier, L.; Massiot, D. *Geochim. Cosmochim. Acta* **2004**, *68*, 5071.

(18) de Lacaillerie, J. B. D.; Fretigny, C.; Massiot, D. *J. Magn. Reson.* **2008**, *192*, 244.
(19) Czjzek, G.; Fink, J.; Gotz, F.; Schmidt, H.; Coey, J. M. D.; Rebouillat, J. P.; Lienard, A. *Phys. Rev. B: Condens. Matter* **1981**, *23*, 2513.
(20) The exhcange rate is given by $k = \pi(W - W_0)$, where W is the width under exchange and W_0 is the instrumental line width in the absence of exchange. We have used the temperature variation of the Na acetate standard as this nonexchange line width.
(21) The variation of the exchange rates with temperature were fit to $k = (k_B T)/(h)\, e^{-\Delta G^{\ddagger}/RT}$, where $\Delta G^{\ddagger} = \Delta H^{\ddagger} - T\Delta S^{\ddagger}$.
(22) Muller, A.; Zhou, Y. S.; Bogge, H.; Schmidtmann, M.; Mitra, T.; Haupt, E. T. K.; Berkle, A. *Angew. Chem., Int. Ed.* **2006**, *45*, 460.
(23) Ziv, A.; Grego, A.; Kopilevich, S.; Zeiri, L.; Miro, P.; Bo, C.; Muller, A.; Weinstock, I. A. *J. Am. Chem. Soc.* **2009**, *131*, 6380.
(24) Petina, O.; Rehder, D.; Haupt, E. T. K.; Grego, A.; Weinstock, I. A.; Merca, A.; Bogge, H.; Szakacs, J.; Muller, A. *Angew. Chem., Int. Ed.* **2011**, *50*, 410.
(25) Merca, A.; Haupt, E. T. K.; Mitra, T.; Bogge, H.; Rehder, D.; Muller, A. *Chem.-Eur. J.* **2007**, *13*, 7650.
(26) Balogh, E.; Anderson, T. M.; Rustad, J. R.; Nyman, M.; Casey, W. H. *Inorg. Chem.* **2007**, *46*, 7032.
(27) Black, J. R.; Nyman, M.; Casey, W. H. *Geochim. Cosmochim. Acta* **2006**, *70*, A53.
(28) Liu, G.; Liu, T. B.; Mal, S. S.; Kortz, U. *J. Am. Chem. Soc.* **2006**, *128*, 10103.
(29) Ettedgui, J.; Neumann, R. *J. Am. Chem. Soc.* **2009**, *131*, 4.
(30) Villa, E. M.; Ohlin, C. A.; Balogh, E.; Anderson, T. M.; Nyman, M. D.; Casey, W. H. *Angew. Chem., Int. Ed.* **2008**, *47*, 4844.
(31) Villa, E. M.; Ohlin, C. A.; Rustad, J. R.; Casey, W. H. *J. Am. Chem. Soc.* **2009**, *131*, 16488.